ChemComm



COMMUNICATION

View Article Online
View Journal | View Issue



Cite this: *Chem. Commun.,* 2018, **54**, 9055

Received 14th May 2018, Accepted 22nd July 2018

DOI: 10.1039/c8cc03869d

rsc.li/chemcomm

Precursors for PbTe, PbSe, SnTe, and SnSe synthesized using diphenyl dichalcogenides†

Zhongyong Wang, Yuanyu Ma, Prathamesh B. Vartak and Robert Y. Wang 0 *

We create precursors for PbTe, PbSe, SnTe, and SnSe by reacting Pb or Sn with diphenyl dichalcogenides in a variety of different solvents. We then deposit $PbSe_xTe_{1-x}$ thin films using these precursors and measure their thermoelectric properties. Introducing Na-dopants into the films allows the thermoelectric properties to be varied.

Solution processing and deposition of inorganic semiconductors enables cost reductions and novel device structures. Recognizing this potential, researchers have applied this approach to the photovoltaic, transistor, 2-5 phase change memory, 6,7 and thermoelectric^{8–10} fields. However, creating solution-processable routes to inorganic semiconductors is non-trivial because inorganic semiconductors are generally insoluble due to their strong covalent bonds. As one exception, hydrazine is known to form soluble metal chalcogenide precursors (SnS₂, In₂Se₃, Cu₂S, etc.)2,11,12 when mixed with metal chalcogenides and excess chalcogen. Unfortunately, hydrazine is problematic for widespread use due to its highly toxic, explosive, and carcinogenic nature. To circumvent this problem, diamine-dithiol solvent mixtures were discovered to readily dissolve a large variety of metal chalcogenides.¹³ However, this binary solvent mixture poses other hurdles. The presence of thiol in the solvent mixture introduces sulfur contamination in metal selenides and tellurides. 9,13 In addition, attempts to create metal tellurides using these hydrazine¹⁴ and thiol-amine solvent¹⁵ approaches often result in a heterogeneous product that contains both metal telluride and free tellurium, unless taken to extra high temperatures. For example, the hydrazine-prepared 14 precursor for PbTe yields a mixture of PbTe and Te unless annealed at 500 °C (note that the melting temperature of Te is 450 °C). While this approach can yield a pure PbTe product, these high temperatures would be problematic for deposition onto organic

School for Engineering of Matter, Transport & Energy, Arizona State University, Tempe, AZ 85287, USA. E-mail: rywang@asu.edu

substrates, such as high temperature plastics for flexible electronics. This problem of free tellurium is also observed when decomposing dithiol–diamine-based precursors. The SnTe precursor made by Webber *et al.*¹⁵ yielded a two-phase mixture of SnTe and Te. These potential sulfur and/or free tellurium contaminants make it difficult to produce impurity-free and phase-pure metal selenides and tellurides using existing precursor methods.

In this work, we propose a new approach to make metal chalcogenide precursors that simultaneously avoids hazardous solvents and eliminates unwanted sulfur and/or tellurium impurities. This approach is also solvent-flexible and does not require special thiol–amine solvent mixtures. Our approach also yields lead selenide and lead telluride precursors, which have been problematic via other precursor syntheses. 16,17 We note that McCarthy et al. 17 prepared a PbTe precursor by mixing PbO-based and Te-based precursors, but that their study also indicated immediate precipitation upon mixing. Lead selenide and telluride precursors are particular appealing because these materials have excellent thermoelectric properties. 18 To showcase this application, we use our precursors to create PbSe $_x$ Te $_{1-x}$ thin films with varying amounts of Na-doping and report their thermoelectric properties.

Fig. 1a shows SnSe, PbSe, SnTe, PbTe, and PbSe $_x$ Te $_{1-x}$ precursors formed in ethylenediamine (EDA) with post-filtering concentrations of 12.8 wt%, 15.8 wt%, 11.0 wt%, 7.8 wt% and 12.0 wt%, respectively (Table S1, ESI†). This reaction can also be done in other solvents such as dimethyl sulfoxide (DMSO), butylamine, and pyridine (Fig. 1b and Fig. S1, ESI†). To perform this reaction, diphenyl diselenide and/or diphenyl ditelluride were first dissolved in one of the abovementioned solvents and then Sn or Pb powder was subsequently added. The molar ratio of diphenyl dichalcogenide to metal was maintained at 1:1. All precursor syntheses were conducted in a nitrogen filled glovebox (see ESI† for a detailed precursor synthesis description).

We believe that cleavage of the chalcogen-chalcogen bond in the diphenyl dichalcogenide molecule by Pb or Sn facilitates

[†] Electronic supplementary information (ESI) available: Experimental procedures, details, and discussion for sample synthesis and characterization, Fig. S1–S8, Scheme S1, and Tables S1–S5. See DOI: 10.1039/c8cc03869d

Communication ChemComm

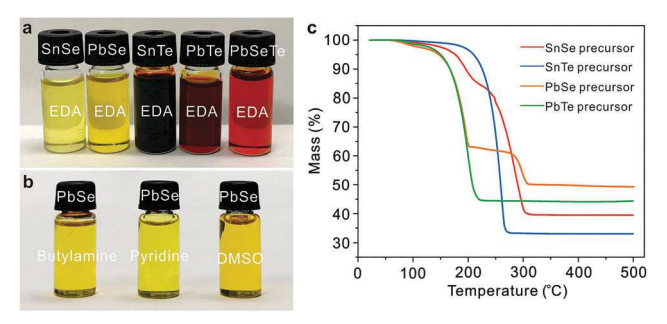


Fig. 1 (a) Photograph of as-synthesized SnSe, PbSe, SnTe, PbTe and PbSe_xTe_{1-x} precursors in ethylenediamine (EDA) solvent as shown from left to right; (b) photograph of as-synthesized PbSe precursors in butylamine, pyridine and dimethyl sulfoxide (DMSO) solvent, respectively, as shown from left to right; (c) thermogravimetric analysis of the SnSe, SnTe, PbSe and PbTe precursors prepared in EDA and carried out at a temperature ramp rate of 2 °C min⁻¹ and conducted in a helium atmosphere.

precursor formation. We verified this via control experiments that substituted diphenyl chalcogenide for diphenyl dichalcogenide (which do not have and do have a chalcogen-chalcogen bond, respectively). When performing synthesis with diphenyl chalcogenide, no precursor formation was observed, thus verifying that the chalcogen-chalcogen bond is the key reaction site.

We also evaluated the precursor stabilities against air and light exposure (Table S2, ESI†). In general, the precursors are insensitive to light, but sensitive to air. When in a nitrogen environment, the PbSe, SnSe and SnTe precursors were stable for the entire duration of our study (e.g. months). However, the PbTe and PbSe_xTe_{1-x} precursors exhibited precipitation in a nitrogen environment after 12 h and 90 h, respectively. Although these PbTe and PbSe_xTe_{1-x} precursor shelf lives are not exceptionally long, they are sufficient to utilize the precursors (all PbTe and PbSe_xTe_{1-x} work in this paper was performed within 2-3 hours after synthesis).

The temperature needed to recover inorganic metal chalcogenide semiconductor from the precursor was identified using thermogravimetric analysis (TGA, Fig. 1c). This analysis shows that the thermal decomposition process finishes at approximately 300 °C, 300 °C, 260 °C, and 210 °C for the SnSe, PbSe, SnTe, and PbTe precursors, respectively. These decomposition temperatures are notably mild, which makes these precursors compatible with flexible substrates such as high temperature plastics (e.g. kapton). Powder X-ray diffraction (XRD) was used to determine the crystal structure of the recovered solids after thermal decomposition of the precursors. Fig. 2 demonstrates that phase-pure SnSe (orthorhombic), PbSe (cubic), SnTe (cubic), PbTe (cubic) are recovered upon decomposition. XRD shows that phase-pure metal chalcogenide products are also recovered when the precursors are prepared in other solvents (Fig. S2, ESI†).

We also mixed our precursors to create metal chalcogenide alloys. Fig. 3 illustrates the creation of $PbSe_xTe_{1-x}$ created by mixing PbSe and PbTe precursors. One promising application for this precursor synthesis is thermoelectricity because PbSe_xTe_{1-x} is among the best performing thermoelectric materials. 19,20 Fig. 3a shows the XRD of our PbSe_xTe_{1-x} samples, with values

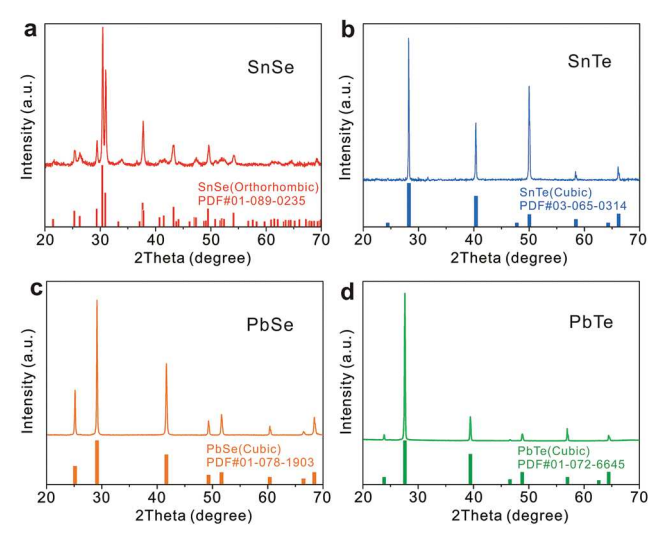


Fig. 2 X-ray diffraction patterns of products recovered from (a) SnSe, (b) PbSe, (c) SnTe and (d) PbTe precursors prepared in ethylenediamine and after annealing at 400 °C for 2 h.

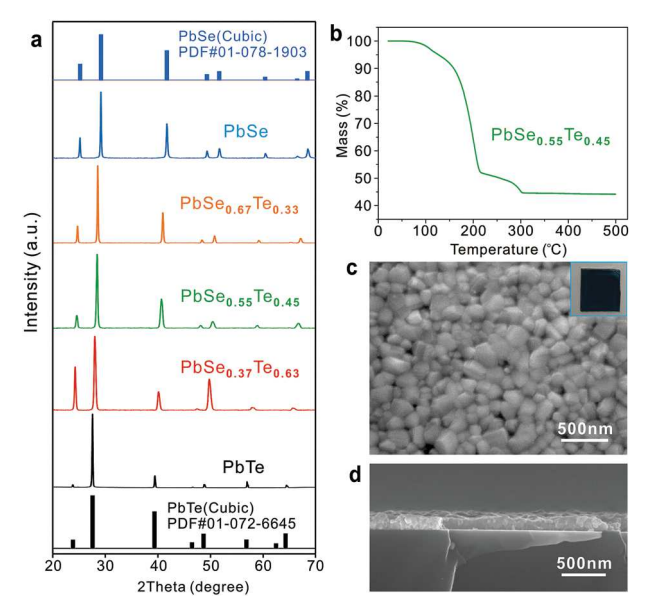


Fig. 3 (a) X-ray diffraction pattern (XRD) of products recovered from $\label{eq:pbSexTe} PbSe_xTe_{1-x} \ precursors \ prepared \ in \ ethylenediamine \ and \ after \ annealing$ at 400 °C for 2 h as well as a comparison with XRD patterns of PbTe and PbSe. (b) TGA of the PbSe $_{0.55}$ Te $_{0.45}$ precursor; (c) top view and (d) cross-sectional view SEM images of a PbSe_{0.55}Te_{0.45} thin film deposited by spin-coating and annealing the PbSe_{0.55}Te_{0.45} precursor on a quartz substrate. The inset in (c) is a PbSe_{0.55}Te_{0.45} thin film deposited on a 1×1 cm quartz substrate.

of x ranging from 0.37–0.63 as determined by energy dispersive X-ray spectroscopy (EDS, Table S3, ESI†). In accordance with Vegard's law, the diffraction peaks of the PbSe_xTe_{1-x} adapt the cubic arrangement of PbSe and PbTe, with peak positions shifting closer to the PbSe locations as the Se concentration is increased. Fig. S3 (ESI†) shows that the lattice parameter and unit cell volume depend linearly on composition and confirm that the $PbSe_xTe_{1-x}$ samples are solid solutions.

Table 1 RBS and profilometry test results of PbSe_xTe_{1-x} and Na-doped PbSe_xTe_{1-x} thin films

ChemComm

Doping level	Pb (%)	те (%)	Se (%)	Thickness (nm)
Undoped	51 ± 5.1	21 ± 2.1	28 ± 2.8	148 ± 9
Lightly-doped	50 ± 5.0	22 ± 2.2	28 ± 2.8	145 ± 4
Moderately-doped	49 ± 4.9	22 ± 2.2	28 ± 2.8	145 ± 2

We used TGA, scanning electron microscopy (SEM), Rutherford backscattering spectroscopy (RBS), and X-ray photoelectron spectroscopy (XPS) to more carefully characterize the PbSe $_{0.55}$ Te $_{0.45}$ precursor and its decomposition product. Fig. 3b shows the TGA analysis of room temperature dried PbSe $_{0.55}$ Te $_{0.45}$ precursor and indicates that decomposition is complete at approximately 300 $^{\circ}$ C.

This precursor can also be spin-coated onto substrates and annealed to produce uniform and continuous thin films. RBS measurements were used to accurately characterize film stoichiometry and revealed a PbSe_{0.56}Te_{0.44} composition (coincidentally, our initial and less accurate EDS measurement gave reasonable results). Table 1 summarizes the RBS measurements along with profilometry results for film thicknesses (see Fig. S5 and S6, ESI† for raw data). Film thickness can be adjusted via spin coating speed and/or precursor concentration (Table S4, ESI†). Fig. 3c and d show top and cross-sectional SEM views of a PbSe_{0.55}Te_{0.45} film along with an optical image (inset). The thin film is composed of densely-packed grains with sizes ranging from approximately 100 nm to 250 nm. A slight increase in grain size was observed as the Te content in the film increased (Fig. S4, ESI†). Attempts to spin coat and anneal pure PbSe or PbTe precursors led to island-like growth.

XPS was used to provide a deeper understanding of our PbSe_{0.56}Te_{0.44} films by providing both the chemical content and chemical electronic state at the film surface. Our XPS analysis indicates the presence of Pb-O and Te-O bonds, but no Se-Se, Te-Te or Pb-Pb binding is observed. Although the presence of surface oxide indicates that our samples are not 100% PbSe_xTe_{1-x}, we attribute this to air exposure during sample transport from our glovebox to the XPS instrument (note that our chemical reagents of Pb, diphenyl diselenide, diphenyl ditelluride, and EDA do not contain oxygen). Surface oxides like this have been reported in other works as well. 21,22 Fig. S7a-e (ESI†) shows our XPS wide scan and high-resolution scans in the Pb 4f, Se 3d, Te 3d, and O 1s regions. We assign peaks at 142.3 eV ($4f_{5/2}$) and 137.4 eV ($4f_{7/2}$) to Pb2+ in PbSe_{0.56}Te_{0.44} and peaks at 143.2 eV (4f_{5/2}) and 138.5 eV $(4f_{7/2})$ to Pb²⁺ in PbO. We assign peaks at 54 eV and 53.3 eV to $3d_{3/2}$ and $3d_{5/2}$ peaks of Se^{2-} in $PbSe_{0.56}Te_{0.44}$, respectively. The $3d_{3/2}$ and $3d_{5/2}$ peaks of Te^{2-} in PbSe $_{0.56}Te_{0.44}$ appear at binding energies of 582.5 eV and 572 eV, respectively. We also observe another two Te $3d_{3/2}$ and Te $3d_{5/2}$ peaks at 586.2 eV and 575.8 eV, which correspond to TeO₂ near the film surface.²³ Lastly, we observe binding energies of 529.5 eV and 530.4 eV in the O 1s region, which correspond to O-Pb and O-Te, respectively. Our binding energy results match well with previous literature data²⁴⁻²⁶ on PbSe_xTe_{1-x} alloys or similar materials (see Table S5, ESI† for direct comparisons to literature data). The Se/Te ratio was also extracted from the XPS wide scan and was in agreement with our RBS results (Table S6, ESI†).

Since $PbSe_xTe_{1-x}$ is a high performance thermoelectric material, we next measured the electrical conductivity and Seebeck coefficient (also known as thermopower) of our $PbSe_{0.56}Te_{0.44}$ films. Dopants also play a key role in thermoelectrics and Na is a common dopant in lead chalcogenide thermoelectrics.²⁷ Consequently, we also sought to include Na dopants in our $PbSe_{0.56}Te_{0.44}$ samples. We introduced Na dopants into our films by adding Na_2S into our precursor mixture (see ESI^{\dagger}) to create lightly Na-doped and moderately Na-doped $PbSe_{0.56}Te_{0.44}$ samples. RBS (Table 1) and XPS (Fig. S7, ESI^{\dagger}) show that our introduction of Na-dopants does not have a significant impact on the Se: Te ratio of the films.

We used secondary-ion mass spectroscopy (SIMS) depth profiling to confirm the presence of Na-dopants in our films (we note that the Na concentration was too dilute to be detected by RBS or XPS). Assuming that the Pb concentration is equivalent in all three samples, we normalized the SIMS Na-signal with the Pb-signal to obtain relative Na concentrations for our samples. Fig. 4 shows the depth profiles of the relative Na-concentration in our undoped, lightly Na-doped, and moderately Na-doped samples (see Fig. S8, ESI† for raw data). As expected, the Na concentration increases as the amount of Na₂S was increased in the precursor mixture. Three regions are observed in these depth profiles (film surface, film interior, and substrate), and the location of the film/Si-substrate interface position was confirmed by profilometry. We hypothesize that the non-uniform Na-distributions in the near-surface region of the film are due to a combination of Na-diffusion²⁸ and/or Na-contamination from the external environment.²⁹

Fig. 5 shows the electrical conductivity and Seebeck Coefficient of the undoped and Na-doped PbSe $_{0.56}$ Te $_{0.44}$ thin films at room temperature. As Na-doping increases the Seebeck coefficient increases from $\sim 480~\mu V~K^{-1}$ to $\sim 630~\mu V~K^{-1}$. The electrical conductivity exhibits the opposite trend. As Na-doping increases, the electrical conductivity decreases from $\sim 180~S~m^{-1}$

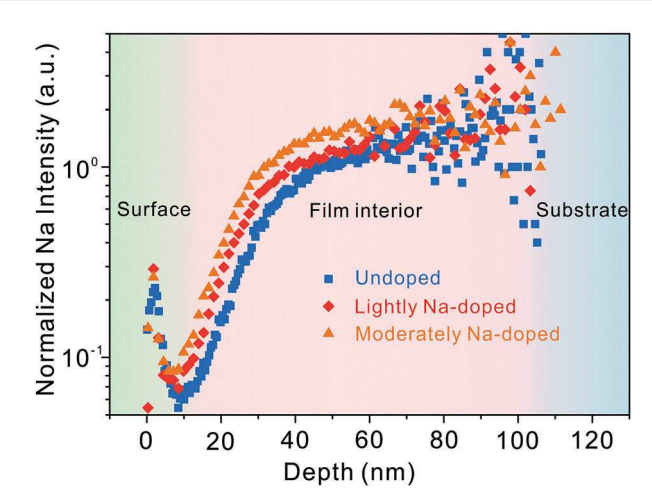


Fig. 4 Second ion mass spectroscopy (SIMS) characterization on undoped and Na-doped PbSe $_{0.56}$ Te $_{0.44}$ thin films deposited on silicon substrates. Elemental depth profiles obtained for Na concentrations are shown for undoped (blue), lightly Na-doped (red) and moderately Na-doped (yellow) films. The y-axis indicates the Na concentration normalized against the Pb concentration.

Communication ChemComm

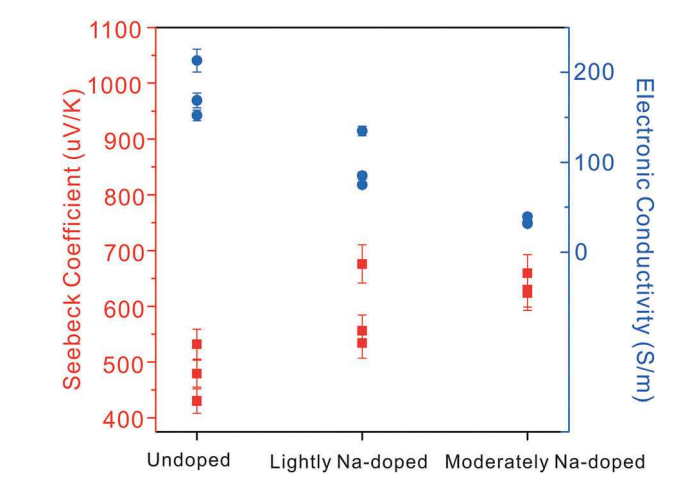


Fig. 5 Room temperature properties of (a) electrical conductivity and (b) Seebeck coefficient of our PbSe $_{0.56}$ Te $_{0.44}$ thin films that are undoped, lightly Na-doped, and moderately Na-doped. Each data point and error bar represent a distinct sample and the corresponding measurement uncertainty on that sample. Many of the error bars for electrical conductivity are smaller than the data point size.

to $\sim\!40~{\rm S~m}^{-1}$. The repeatability of our synthesis procedures is confirmed by the fact that the Fig. 5 data were derived from 3 different samples at each doping level and prepared from 3 separate batches of PbSe_{0.56}Te_{0.44} precursor.

The positive value of the Seebeck coefficient indicates that our PbSe_{0.56}Te_{0.44} films are p-type. The increase in Seebeck coefficient and decrease in electrical conductivity as Na-doping increases suggests that Na-doping is decreasing the hole concentration (i.e. that Na-doping is moving the Fermi level away from the valence band edge). We hypothesize that our observed Na doping effect can be explained by the existence of lead vacancies in our undoped samples and a preference for the Na dopants to occupy these vacancy sites (see ESI† for more discussion). Thermal conductivity is another important thermoelectric property and we anticipate that the nanograins, nanoporosity, and alloyed elements in our samples will lead to low thermal conductivities via phonon scattering. 20,30 Although PbSe_xTe_{1-x} is one of the best performing thermoelectric materials, its room temperature performance is quite low. PbSe_rTe_{1-r} thermoelectrics are best-suited for electricity generation from heat sources at temperatures above 600 K.30 Consequently, future high temperature thermoelectric measurements on our films could be interesting.

In conclusion, we reported a new route to make PbSe, PbTe, SnSe, SnTe, and PbSe_xTe_{1-x} precursors by reacting Pb and Sn with diphenyl diselenide and/or diphenyl ditelluride in a variety of solvents. Compared to the hydrazine and diamine–dithiol routes, our approach is solvent-flexible, utilizes safe solvents, and avoids sulfur impurities. These precursors also access PbSe, PbTe, and PbSe_xTe_{1-x} compositions, which have been historically difficult to make. We also used these precursors to deposit thin films of undoped and Na-doped PbSe_xTe_{1-x} and reported their thermoelectric properties.

This work was supported by the National Science Foundation through award number DMR-1506829. We acknowledge

the use of facilities within the Eyring Materials Center at Arizona State University. We also thank Mark Mangus and Lynda Williams for RBS and SIMS analysis, respectively.

Conflicts of interest

There are no conflicts to declare.

Notes and references

- D. B. Mitzi, M. Yuan, W. Liu, A. J. Kellock, S. J. Chey, V. Deline and A. G. Schrott, *Adv. Mater.*, 2008, 20, 3657–3662.
- 2 D. B. Mitzi, L. L. Kosbar, C. E. Murray, M. Copel and A. Afzali, Nature, 2004, 428, 299–303.
- 3 D. Kim, Y. Jeong, K. Song, S. K. Park, G. Z. Cao and J. Moon, Langmuir, 2009, 25, 11149–11154.
- 4 S. T. Meyers, J. T. Anderson, C. M. Hung, J. Thompson, J. F. Wager and D. A. Keszler, *J. Am. Chem. Soc.*, 2008, **130**, 17603–17609.
- 5 M. M. Lee, J. Teuscher, T. Miyasaka, T. N. Murakami and H. I. Snaith. Science, 2012, 338, 643-647.
- 6 D. J. Milliron, S. Raoux, R. Shelby and J. Jordan-Sweet, *Nat. Mater.*, 2007, 6, 352–356.
- 7 R. Y. Wang, M. A. Caldwell, R. G. D. Jeyasingh, S. Aloni, R. M. Shelby, H. S. P. Wong and D. J. Milliron, *J. Appl. Phys.*, 2011, **109**, 113506.
- 8 R. Y. Wang, J. P. Feser, X. Gu, K. M. Yu, R. A. Segalman, A. Majumdar, D. J. Milliron and J. J. Urban, *Chem. Mater.*, 2010, 22, 1943–1945.
- 9 Y. Ma, P. B. Vartak, P. Nagaraj and R. Y. Wang, RSC Adv., 2016, 6, 99905–99913.
- 10 Z. Lin, C. Hollar, J. S. Kang, A. Yin, Y. Wang, H. Y. Shiu, Y. Huang, Y. Hu, Y. Zhang and X. Duan, Adv. Mater., 2017, 29, 1606662.
- 11 D. B. Mitzi, M. Copel and S. J. Chey, Adv. Mater., 2005, 17, 1285-1289.
- 12 D. B. Mitzi, Inorg. Chem., 2007, 46, 926-931.
- 13 D. H. Webber and R. L. Brutchey, *J. Am. Chem. Soc.*, 2013, 135, 15722–15725.
- 14 H. Zhang, J. S. Son, D. S. Dolzhnikov, A. S. Filatov, A. Hazarika, Y. Y. Wang, M. H. Hudson, C. J. Sun, S. Chattopadhyay and D. V. Talapin, *Chem. Mater.*, 2017, 29, 6396–6404.
- 15 D. H. Webber, J. J. Buckley, P. D. Antunez and R. L. Brutchey, *Chem. Sci.*, 2014, 5, 2498–2502.
- 16 C. L. McCarthy and R. L. Brutchey, Chem. Commun., 2017, 53, 4888–4902.
- 17 C. L. McCarthy, D. H. Webber, E. C. Schueller and R. L. Brutchey, Angew. Chem., Int. Ed., 2015, 54, 8378–8381.
- 18 H. Wang, Y. Z. Pei, A. D. LaLonde and G. J. Snyder, Adv. Mater., 2011, 23, 1366–1370.
- 19 Y. Z. Pei, X. Y. Shi, A. LaLonde, H. Wang, L. D. Chen and G. J. Snyder, Nature, 2011, 473, 66–69.
- 20 P. F. P. Poudeu, J. D'Angelo, H. J. Kong, A. Downey, J. L. Short, R. Pcionek, T. P. Hogan, C. Uher and M. G. Kanatzidis, *J. Am. Chem.*
- Soc., 2006, 128, 14347–14355.21 D. B. Mitzi, M. Copel and C. E. Murray, Adv. Mater., 2006, 18, 2448–2452.
- 22 Q. A. Zhang, T. Sun, F. Cao, M. Li, M. H. Hong, J. K. Yuan, Q. Y. Yan, H. H. Hng, N. Q. Wu and X. G. Liu, *Nanoscale*, 2010, 2, 1256–1259.
- 23 U. Nithiyanantham, M. F. Ozaydin, A. S. Tazebay and S. Kundu, New J. Chem., 2016, 40, 265–277.
- 24 X. G. Sun, K. W. Gao, X. L. Pang, H. S. Yang and A. A. Volinsky, J. Mater. Sci.: Mater. Electron., 2016, 27, 1670–1678.
- 25 X. G. Sun, K. W. Gao, X. L. Pang, H. S. Yang and A. A. Volinsky, J. Mater. Sci.: Mater. Electron., 2015, 26, 7873–7881.
- 26 J. Song, W. Feng, Y. Ren, D. Zheng, H. Dong, R. Zhu, L. Yi and J. Hu, Vacuum, 2018, 155, 1–6.
- 27 J. Q. He, L. D. Zhao, J. C. Zheng, J. W. Doak, H. J. Wu, H. Q. Wang, Y. Lee, C. Wolverton, M. G. Kanatzidis and V. P. Dravid, *J. Am. Chem. Soc.*, 2013, 135, 4624–4627.
- 28 A. Yamini, T. Li, D. R. G. Mitchell and J. M. Cairney, *Nano Energy*, 2016, 26, 157–163.
- 29 I. Constant, F. Tardif and J. Derrien, Semicond. Sci. Technol., 2000, 15. 61–66.
- 30 L. D. Zhao, V. P. Dravid and M. G. Kanatzidis, Energy Environ. Sci., 2014, 7, 251–268.